Accepted Manuscript

Title: Analysis of Loads, Temperatures and Welds Morphology in FSW of Polycarbonate

Authors: F. Lambiase, A. Paoletti, V. Grossi, A. Di Ilio

PII: S0924-0136(18)30531-4
DOI: https://doi.org/10.1016/j.jmatprotec.2018.11.043
Reference: PROTEC 16036

To appear in: *Journal of Materials Processing Technology*

Received date: 4 August 2018
Revised date: 19 November 2018
Accepted date: 27 November 2018

Please cite this article as: Lambiase F, Paoletti A, Grossi V, Di Ilio A, Analysis of Loads, Temperatures and Welds Morphology in FSW of Polycarbonate, *Journal of Materials Processing Tech.* (2018), https://doi.org/10.1016/j.jmatprotec.2018.11.043

This is a PDF file of an unedited manuscript that has been accepted for publication. As a service to our customers we are providing this early version of the manuscript. The manuscript will undergo copyediting, typesetting, and review of the resulting proof before it is published in its final form. Please note that during the production process errors may be discovered which could affect the content, and all legal disclaimers that apply to the journal pertain.

ACCEPTED MANUSCRIPT

Analysis of Loads, Temperatures and Welds Morphology in FSW of Polycarbonate.

F. Lambiase, A. Paoletti, V. Grossi, A. Di Ilio

Dept. of Industrial and Information Engineering and Economics, University of L'Aquila, via G. Gronchi 18, Zona Industriale di Pile, 67100 (AQ), Italy

*Corresponding author:
F. Lambiase
francesco.lambiase@univaq.it
Monteluco di Roio, 67040 (AQ), Italy
Tel. N.: (+39) 0862 434343
Fax N.: (+39) 0862 434303

Graphical abstract

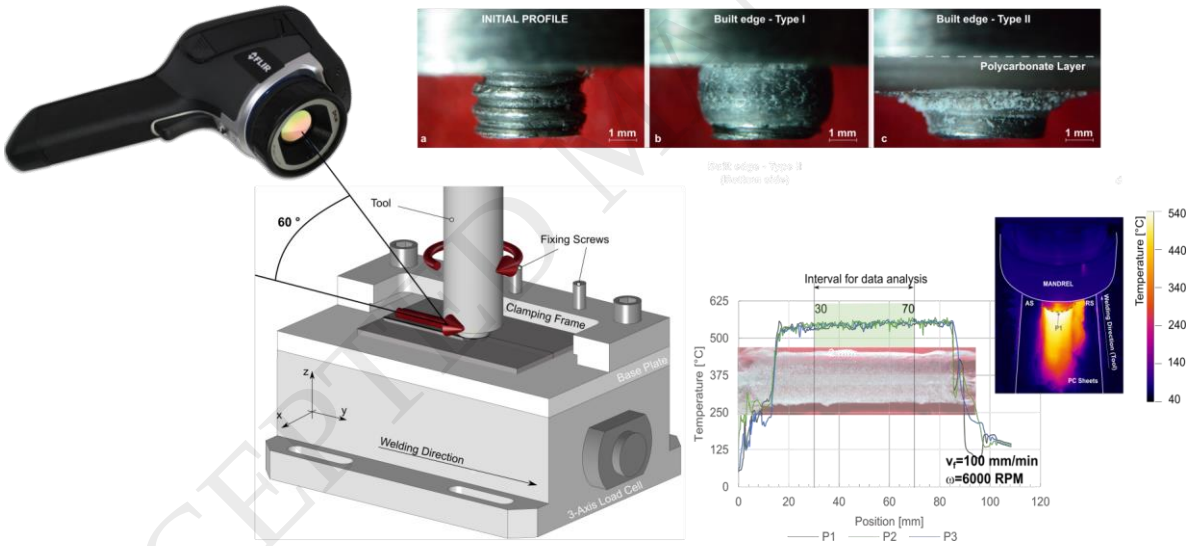

Abstract

The influence of welding and tool rotation speeds on processing loads and temperature distribution developing is Friction Stir Welding of polycarbonate is investigated, experimentally. The development of critical conditions leading to macroscopic defects were correlated to the features of loads and temperature trends. Two macroscopic defects were identified on FSW welds. Under low welding speeds, the welds were characterized by circular rifts. These developed due to unsteady conditions and low contact pressure. High welding speeds involved heavier loads and temperature within the weld seam. This came with the formation of built-up edge (BUE) under the tool shoulder. The BUE induced a "milling action" on the weld path leading to significant thinning of the weld seam. The acquired signals (loads and temperature measurements) revealed the features of the surface morphology. This suggests the possibility to use such measurements to predict (and possibly to avoid) the onset of the aforementioned defects.

ACCEPTED MANUSCRIPT

Keywords: FSW, polymers, temperature analysis, mechanical characterization, processing loads

1. Introduction

Friction Stir Welding of polymers and fiber-reinforced polymers is becoming very popular since the great advantages as compared to conventional joining/welding processes. These include higher productivity, high weld strength, great energy efficiency and absence of subsidiary material, avoidance of pretreatments lading to reduced overall costs.

The quality of FSW joints depends on the geometry of the weld and the morphology and behavior of the stirred and surrounding regions. Obviously, the quality and strength of FSW welds is also affected by induced defects e.g. bubbles development, vacuum voids as well as polymer degradation etc. Elyasi and Derazkola (2018) identified in the shrinkage holes the crack initiation for PMMA welds made by FSW. Lambiase et al. (2017a) reduced the amount of bubbles and vacuum voids in FSSW welds made on polycarbonate by controlling the plunging force. This enabled to improve the strength of the welds significantly. The design of the tool and the selection of the process conditions determine the quality of these welds. Huang et al. (2018) subdivided the influencing parameters of FSW into three categories: geometry of the tool (shoulder and pin dimensions, pin topology), process parameters (tool rotational speed, welding speed, tilt angle and plunging depth) and mechanical and thermal properties of the material/materials.

Preliminary studies concerning FSW of polymers were highly focused on determining the feasibility of the process along with the processing conditions that maximized the strength of the welds. Bozkurt (2012) conducted experimental tests according to an orthogonal array to maximize the tensile strength of FSW welds made on Polyethylene (PE) sheets. Bagheri et al. (2013) followed a similar approach to determine the influence of the process parameters using a hot shoe equipment for ABS sheets. Many subsequent studies followed a similar approach. A deeper analysis of the process is required to understand more in depth how the process develops and how it influences the quality of the joints. More advanced techniques were adopted to determine the influence of the process conditions on the quality, and mechanical behavior of the FSW welds made on thermoplastics. Panneerselvam and Lenin (2014) studied the influence of the tool rotation direction (using a threaded tool) on the welds morphology. The results indicated that clockwise pin rotation produced lower quality welds in terms of cavity and blow holes dimensions and poor adhesion of the stirred zone with the base material. Simoes and Rodrigues (2014) analyzed the material flow and the process conditions during FSW of PMMA. The authors used advanced analysis methods including photo-elasticity and IR thermography to provide a deeper insight into the influence of the process conditions on the quality of the joints. Moreno et al. (2018) studied the influence of the process parameters on the quality of FSW welds made on HDPE by means of stationary shoulder. The joints were analyzed by using: tensile and micro-hardness tests, analysis of the morphology, fracture surface analysis and DSC tests. Mendes et al. (2014a) investigated the influence of process parameters on the strength and morphology of FSW made on ABS. The results reported in this paper from the Digital Image Correlation (DIC) analysis showed a very narrow region where the strain concentrates during the tensile tests. Mendes et al. (2014b) studied the influence of the processing conditions (including the temperature of the hot shoe) on the morphology and strength of ABS sheets. Vijendra and Sharma (2015) investigated the influence of the FSW tool temperature (heated by means of an external inductor) on the HDPE. The authors classified different types of fracture resulting from different processing conditions. Derazkola and Simchi (2018a) developed alumina reinforced nanocomposites by means of FSW. The add of alumina increased the tensile and flexural strength as well as the impact energy. Banjare, et al. (2017) studied the influence of external

ACCEPTED MANUSCRIPT

heating (by means of an assisted heating tool) on tensile strength and morphology of PP sheets. The results indicated that the external heating determined a significant increase in the tensile strength, elongation at fracture and better surface finish. Besides process parameter, tool geometry and topology optimization, some authors have tried to improve the mechanical strength of FSW welds by using different filler particles. Azarsa and Mostafapour (2013) found an increase of the Ultimate Tensile Strength (10%) and modulus of elasticity (30%) when copper particles were added to HDPE by means of FSW. Similarly, Gao et al. (2016) used carbon nanotubes to improve the strength of HDPE and ABS welds made by FSW. However, the authors did not compare the strength of the welds made with and without the filler nanotubes.

Measurements of processing loads and temperature variation provide deeper insight into the process evolution, development of steady and unsteady conditions, and the effect of the process parameters. In addition, the analysis of the process loads represents a key aspect for machine design as well as to analyze the effect of process conditions and maybe to forecast the onset of defects. To this end, Eslami et al. (2018) involved a multi-axis load measurements equipment during FSW experimental tests. The results indicated that the load trends provide useful information concerning the onset of some defects. Derazkola and Simchi (2018b) developed a FE model to investigate the influence of the topology of the tool pin on the material flow, temperature distribution and strength of PMMA welds made by FSW. Sahu et al. (2018) analyzed the influence of the process conditions and tool topology (conical, square and conical) on the FSW loads. The literature review points out that great steps forward have been done in terms of characterization of the FSW welds by means of advanced techniques and crossed approaches. However, more work is needed from the side of process analysis as only a few researches have been conducted in this direction.

The present investigation is aimed at understanding the influence of FSW process parameters on processing loads, temperature distribution and morphology of the welds and how these aspects are mutually correlated. Experimental tests were conducted varying the main process parameters, i.e. welding speed, and tool rotation speed, over a wide range of conditions. A CNC machine equipped with a multi-axis load transducer was adopted to acquire the load variation during the process. Temperature measurements were performed by means of an Infrared (IR) camera. Load and temperature trends were crossed with the morphology of the welds. The main macroscopic defects occurring on the welds seam were identified and related to the process conditions.

2. Materials and Methods

Friction Stir Welding experiments were conducted on polycarbonate sheet (LEXAN) of thickness 3 mm. Polycarbonate is an amorphous thermoplastic with relatively high mechanical strength and toughness, good optical transparency and chemical resistance. Differential Scanning Calorimetry (DSC) analysis and Thermogravimetric Analysis (TGA) were conducted to determine the Glass transition Temperature and the degradation temperature, respectively. DSC tests were performed by means of a machine model DSC8500 by Perkin Elmer. TGA tests were conducted on a machine model L81/1550 by LINSEIS. Mechanical characterization of the base material was performed by means of tensile tests, according to ASTM D638 standards. The main mechanical properties of the material are summarized in Table 1.

FSW tests were performed by means of a 3-axis instrumented machine. The bottom plate was fixed to a piezoelectric transducer type 9257B by Kistler, which was connected to a charge amplifier type 5017 by Kistler. The signals were acquired by means of an I/O acquisition

ACCEPTED MANUSCRIPT

board model USB6009 by National Instrument at a sample rate of 100 Hz. Further data analysis was conducted to separate the different force signals into F_x (load in transverse direction), F_y (load in welding direction) and F_z (Clamping load) and M_z. A schematic of the clamping system, coordinate system and load cell is depicted in Fig. 1.

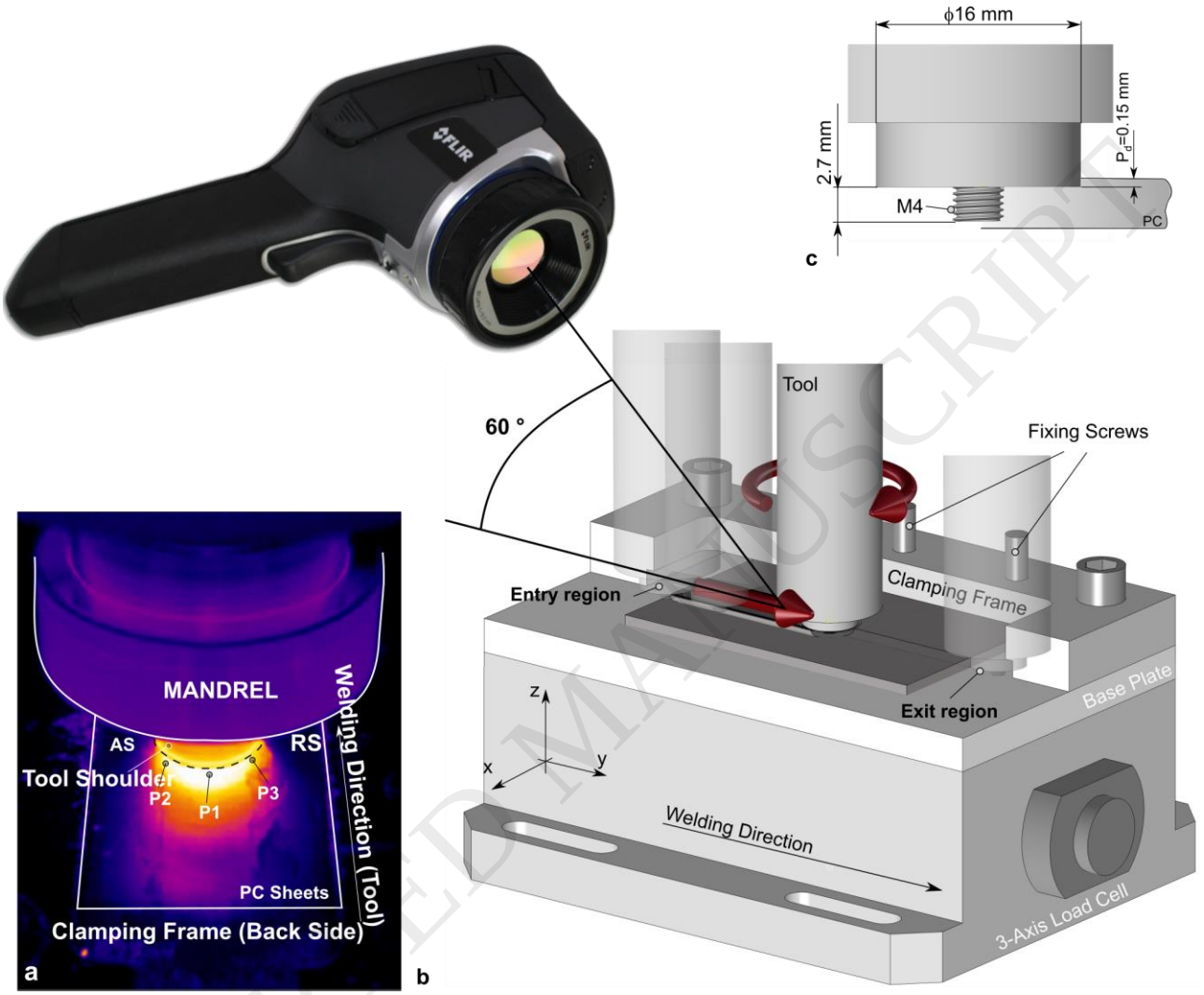

Fig. 1 Schematic of (a) IR image with control points and (b) clamping system, coordinate system, acquisition transducer and (c) tool geometry.

The torque acting on the tool Mz was calculated by means of Eq. (1):

$$M_z = M_{z\,(cell)} - F_x \cdot y \qquad \text{Eq. (1)}$$

where $M_{z(cell)}$ and y represent the torque measured by the load transducer and the y position, respectively. To this end, a linear variable differential transformer (LVDT) was adopted to measure the y position during FSW tests. The knowledge of M_z tool provides information concerning the required torque for machines design, the absorbed power P and the specific energy E_s that is the energy required to produce a weld of unit length (1 mm).

$$P = M_z \cdot \omega + F_y \cdot v_f \cong M_z \cdot \omega \qquad \text{Eq. (2)}$$

$$E_s = P / v_f \qquad \text{Eq. (3)}$$

In Eq. (2) the second term is generally much lower than the contribute of the torque, thus it can be neglected. During the experiments, the temperature distribution was measured by means of an IR camera model E60 by FLIR. The camera was positioned at a distance of

ACCEPTED MANUSCRIPT

almost 300 mm from the tool/material contact region (to measure the temperature behind the tool) with an angle of almost 60 degrees, as shown in Fig. 1. The maximum acquisition rate allowed by the camera (30 Hz) was adopted for the IR analysis. The material emissivity was determined by means of the approach reported by Lambiase et al. (2017b). A heated bed with controlled temperature was used to heat the bottom face of a polycarbonate sample. The temperature of the upper surface was measured by means of a K-Type thermocouple with a response time of 0.5 s. The bed was heated at prescribed temperatures in a stepwise manner. Then, the temperature of the upper surface was measured by means of the thermocouple and the emissivity of the material was computed by the FLIR software, inversely. This procedure was repeated in the range 30-360 °C. Higher temperature measurements were not possible as the heating table limitation as well as great sample distortion and the onset of substantial surface modifications. The temperature evolution was measured on three points (P1, P2 and P3) close to the tool shoulder. These points were chosen in correspondence of: the weld line (P1), the advancing side AS (P2) and the retracting side RS (P3), as shown in Fig. 1.

The specimens were cut from a unique sheet by means of a rotary blade to a dimension of 60 mm × 90 mm (width × length). The joints were produced in butt configuration. The FSW tool was characterized by a shoulder diameter of 16 mm and threated pin M4 × 2.70 mm. These dimensions and the pin length (90% of the thickness of the sheets) were selected on the basis of literature analysis (generally the tool shoulder that is 3-4 larger than the pin is used), and preliminary experiments. The tool was made of C40 steel. Experimental tests were conducted with a plunging depth P_d=0.15 mm and a tilt angle α=0°. Such a value was determined by preliminary experimental tests. The experimental test campaign consisted in the full factorial plan summarized in Table 2. Each experimental condition was replicated three times.

This experimental plan was selected with the aim of extending the normally adopted range of levels used for FSW of thermoplastics. This choice was driven by a more comprehensive understanding of the process as well as to provide useful information at high welding speeds to maximize the process productivity. The quality of the joints was assessed by means of optical microscopy. This end, optical analysis was performed by means of a stereo-microscope model Stemi DV4 by ZEISS equipped with a DSLR camera model D5200 by Nikon. Geometrical characterization of the tool was also performed after each FSW experiment to determine the amount of PC material that adhered to the tool pin and/or under the tool shoulder.

3. Results

3.1 Thermal characteristics of Polycarbonate

DSC analysis indicated that the glass transition temperature of the base material occurred at 152 °C. Fig. 2s depicts the results from the DTA and TGA analyses. These trends indicate a significant polymer degradation development above 400°C (from TGA) along with an endothermic peak (from DTA) at 490 °C.

ACCEPTED MANUSCRIPT

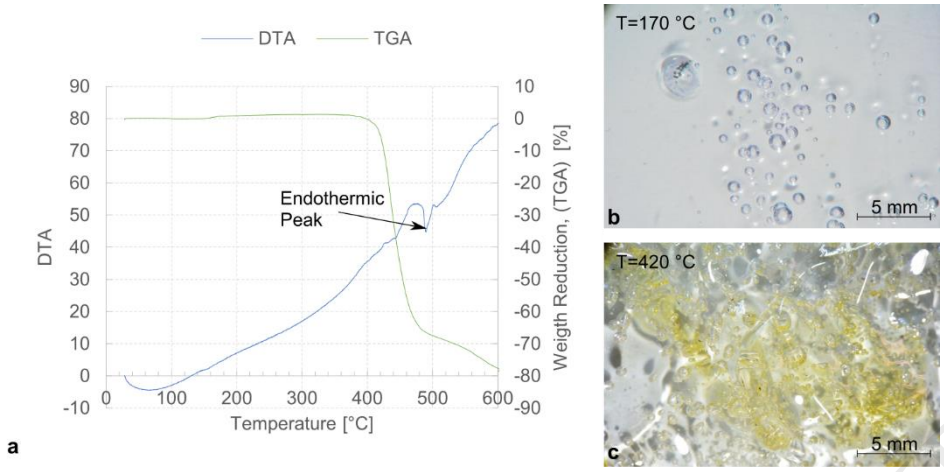

Fig. 2 Thermal and morphological characteristics of the base material. (a) Results from DTA and TGA analyses and surface morphology of samples heated at (b) 170 °C and 420 °C.

Fig. 2b shows the presence of bubbles with dimension ranging between 0.3-1.5 mm when base material is heated up at 170 °C. The onset of these bubbles is due to the moisture content of the polymer, as polycarbonate is highly hygroscopic. On the other hand, raising the temperature over 420°C leads to polymer degradation (from TGA) that comes with a yellowish color of the polycarbonate, as shown in Fig. 2c.

3.2 Material flow

Fig. 3 depicts the macrograph of the upper surface of the samples. Under low welding speeds, unsteady material flow was observed regardless the tool rotation speed. This condition is characterized by the presence of circular rifts released by the tool shoulder at discrete distance (almost 10-11 mm) from each other. These rifts were due to the material reflow from the back of the tool during the process. On the other hand, for high values of v_f, the welds showed a more regular morphology (especially for those produced with ω=6000 RPM), even though they were characterized by large amount of material removal. Under the intermediate level of the tool rotation speed (ω=4000 RPM), steady state conditions developed after a relatively longer unsteady path. The welds produced at the highest tool rotation speed ω=6000 RPM and intermediate welding speed conditions (v_f=40 mm/min and v_f=60 mm/min) showed closer rifts as compared to those observed under lower welding speed (distance of almost 1 mm). In addition, a yellowish color was observed on those joints indicating the onset of thermal degradation within the polymer.

ACCEPTED MANUSCRIPT

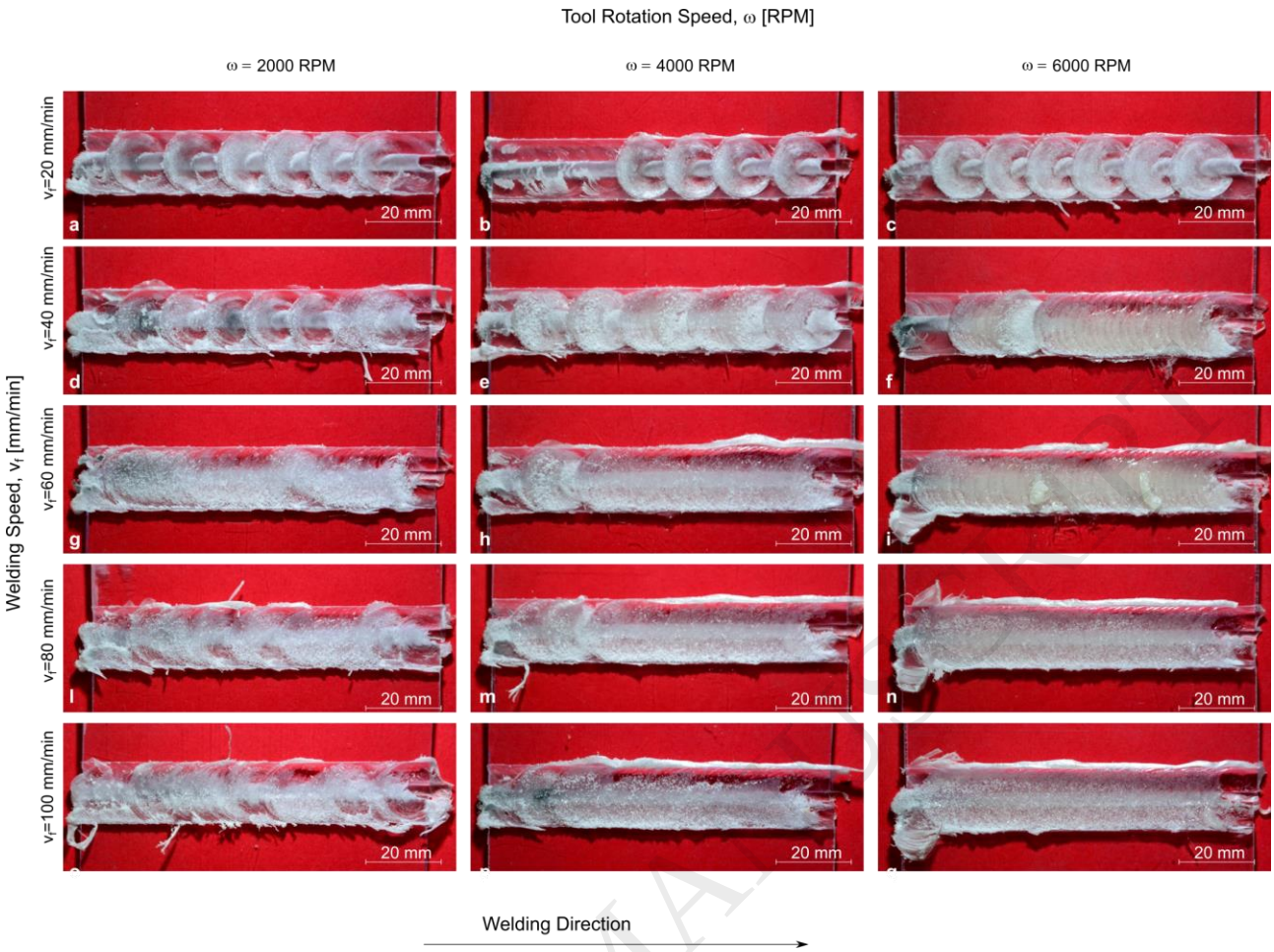

Fig. 3 Upper surface of welds performed under different processing conditions.

Fig. 4a-f depict the macrographs of some reference conditions performed at higher magnification. The aforementioned rifts and the yellowish appearance can be easily distinguished on the surface of the samples welded at v_f=20 mm/min and v_f=40 mm/min, respectively. On the other hand, higher magnification of the samples made under v_f=100 mm/min (Fig. 4c and Fig. 4f) revealed the material removal from the upper surface of the weld seam. This can be more easily observed on the cross section reported in Fig. 4g.

ACCEPTED MANUSCRIPT

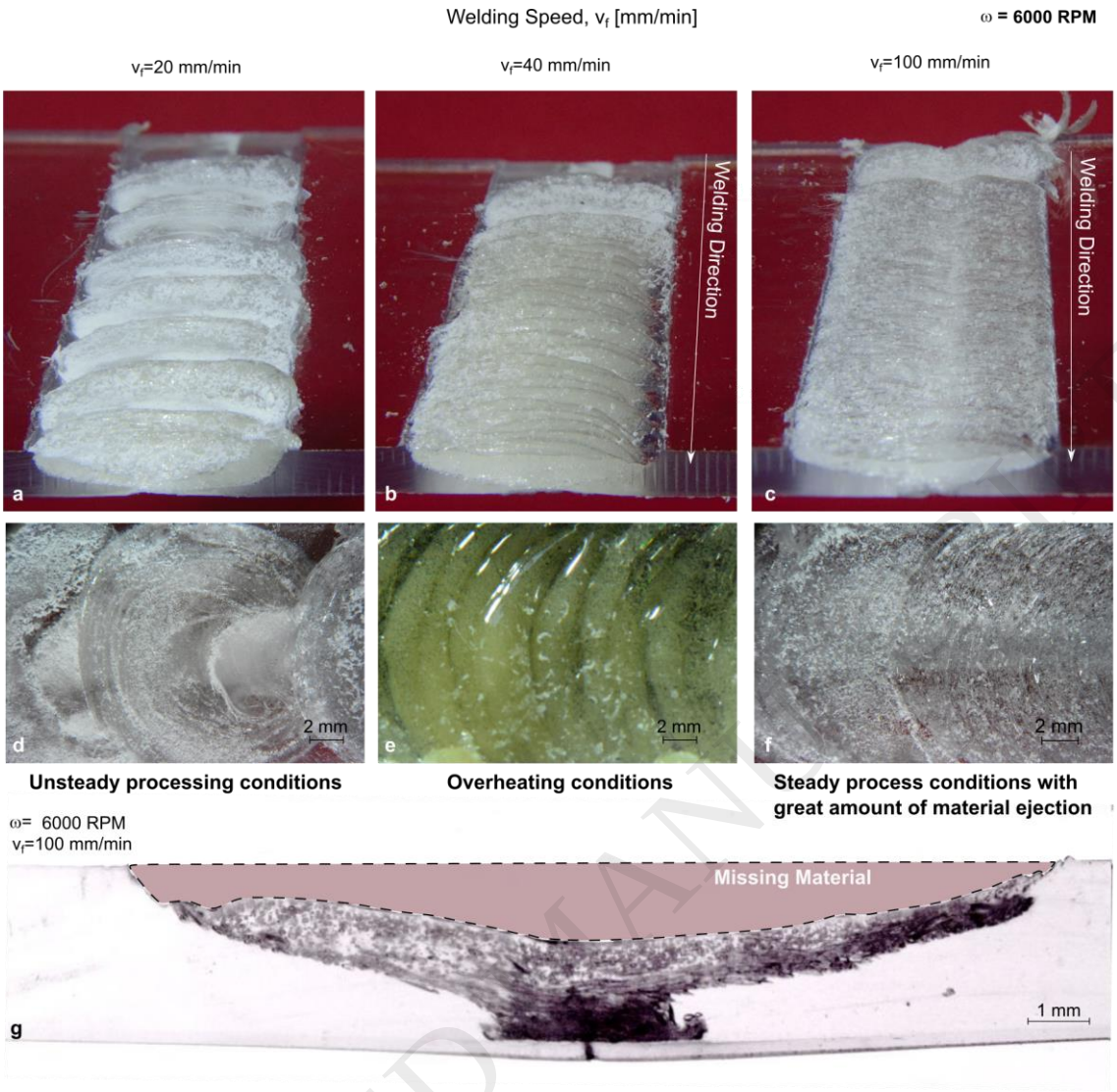

Fig. 4 Typical features of welds.

Before and after each experiment, the tool was observed by means of a stereoscope to better understand the cause of the missing material. Fig. 5a depicts the geometry of the tool, which was restored before each test. Fig. 5b and Fig. 5c reports the side view of the tool after given processing conditions. Both these macrographs show the presence of polycarbonate on the tool. In Fig. 5b, the polycarbonate mainly adhered to the pin. On the other hand, Fig. 5c indicates that in some other cases (summarized in Table 3) a thick layer (up to 1.2 mm) the polycarbonate also adhered underneath the tool shoulder (as better shown in Fig. 5d).

ACCEPTED MANUSCRIPT

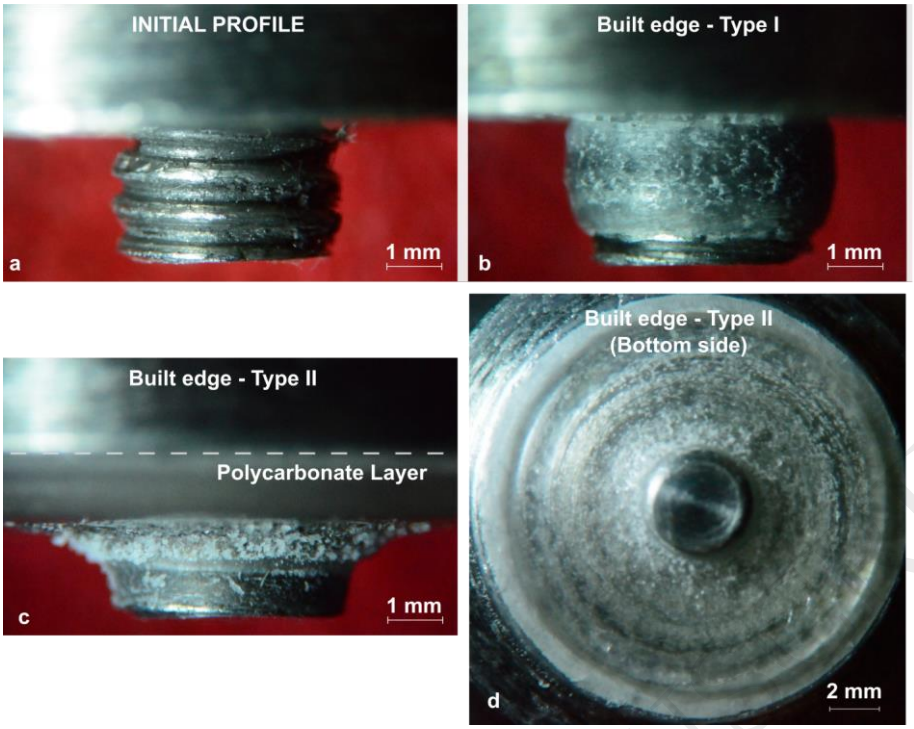

Fig. 5 Side view of the tool pin (a) Initial profile, (b) BUE on the pin, (c) BUE on the pin and under the shoulder and (d) bottom view of the BUE under the tool shoulder.

These pictures clearly indicate the formation of a built-up edge (BUE), which is a common defect of machining processes. The presence of the BUE represents a defect as it modifies the geometry of the tool surface. In addition, the BUE increases the amount of material ejection ahead the tool leading to a "milling action" on the weld surface. This caused the material removal, shown in Fig. 4g. Table 3 summarizes the influence of the processing conditions on the type of BUE observed after each test. When low welding speeds were adopted ($v_f \leq 40$ mm/min), the polycarbonate adhered to the tool pin (BUE type I). On the other hand, higher welding speeds ($v_f \geq 60$ mm/min) involved great quantity of material adhered underneath the tool shoulder (BUE type II), with the exception of ω=2000 RPM.

ACCEPTED MANUSCRIPT

3.3 Processing Loads

3.3.1 Analysis of welding and plunging force

Fig. 6 depicts the processing loads under three processing conditions: v_f=20 mm/min, and (b) v_f=40 mm/min and (c) v_f=100 mm/min. The tool rotation speed is fixed at ω=6000 RPM. As the tool shoulder has completely entered in contact with the sheets (after a path of almost 22-25 mm), steady state conditions are expected. However, for v_f=20 mm/min, both the plunging load (F_z) and the welding load (F_y) undergo frequent rises and drops, as shown in Fig. 6a. For v_f=100 mm/min, the load variation (after the initial transient path) is more limited, as depicted in Fig. 6b. Under this condition, the loads were characterized by frequent oscillations of lower entity. The comparison of load trends and the surface morphology of the welds suggests that the load features such as the load peaks shown in Fig. 6a correspond to the circular rifts observed on the weld surface. Similarly, a smoother and more regular surface correspond to a lower variation of the processing loads, as depicted in Fig. 6b.

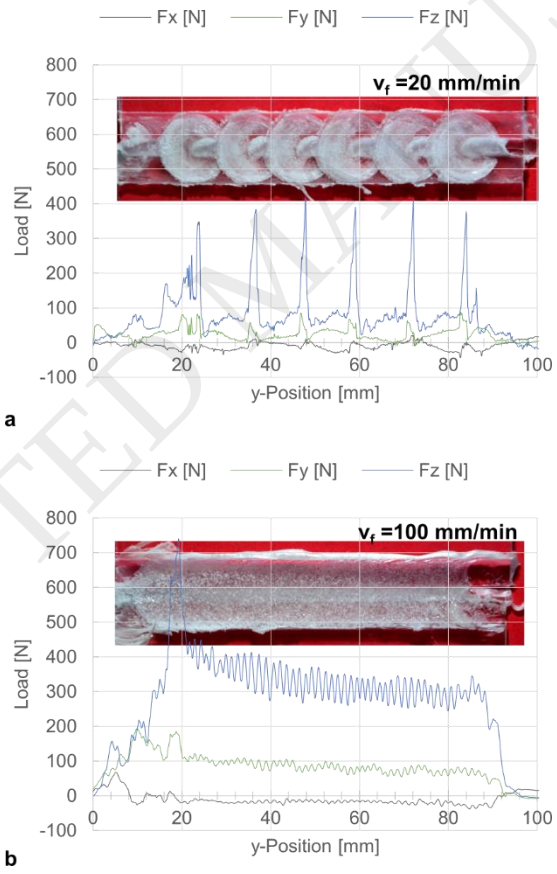

Fig. 6 Variation of main processing forces during FSW (a) v_f=20 mm/min, and (b) v_f=100 mm/min. The tool rotation speed is fixed at ω=6000 RPM.

Fig. 7a-c compare different trends of the plunging load (Fz) varying the process conditions. Low welding speeds generally led to the onset of great load peaks, which are indicative of the circular rifts. Conversely, higher welding speeds produced lower load variations, regardless the tool rotation speed.

ACCEPTED MANUSCRIPT

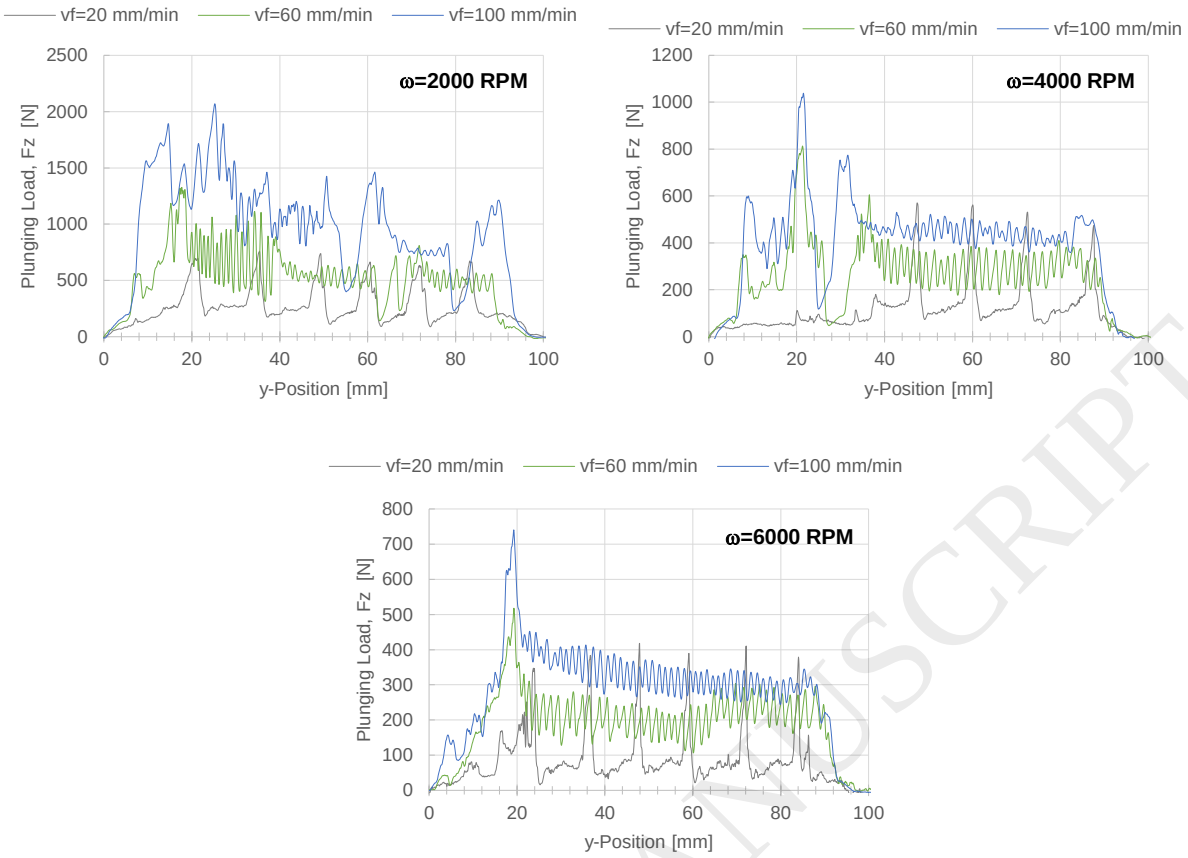

Fig. 7 Comparison of Plunging load varying the welding speed and tool rotation speed (a) ω=2000 RPM; (b) ω=4000 RPM and (c) ω=6000 RPM.

Fig. 8a-b depict the variation of the mean values of the processing loads (calculated between y-position 30 mm-70 mm, named "interval for data analysis") with the process parameters. Higher tool rotation speeds involved lower values of F_y and F_z. Actually, higher tool rotation speed caused higher material temperature and consequently lower interfacial contact shear stress, which caused the reduction of the processing loads. The increase of F_y with the welding speed was due to the increase in the pressure exerted by the polycarbonate (in front of the tool), which was forthcoming to be stirred. This caused an increase in the hydrostatic pressure under the tool that drove the increase of F_z. Under low welding speeds (and high tool rotation speed), F_y held almost constant with a mean value less than 50 N. For ω=6000 RPM, F_y held constant up to v_f=60 mm/min; then, it started to increase for higher welding speeds. A similar trend was observed for ω=4000 RPM, where the threshold was found for v_f=40 mm/min. These trends suggest the existence of a threshold value of the welding speed above which the welding force increased with the welding speed. These behaviors can be explained by considering the state of the material ahead the tool. For relatively low welding speeds, the tool is surrounded by a larger portion of material (given the long interaction time) that is in pasty state. On the contrary, as the welding speed increases, this region becomes much thinner (as the lower interaction time) and induced a higher pressure on the tool. This caused the increase of both F_y and F_z. Thus, higher values of the tool rotation speed involve higher values of the threshold value as higher heat is supplied, as shown in Fig. 8a.

ACCEPTED MANUSCRIPT

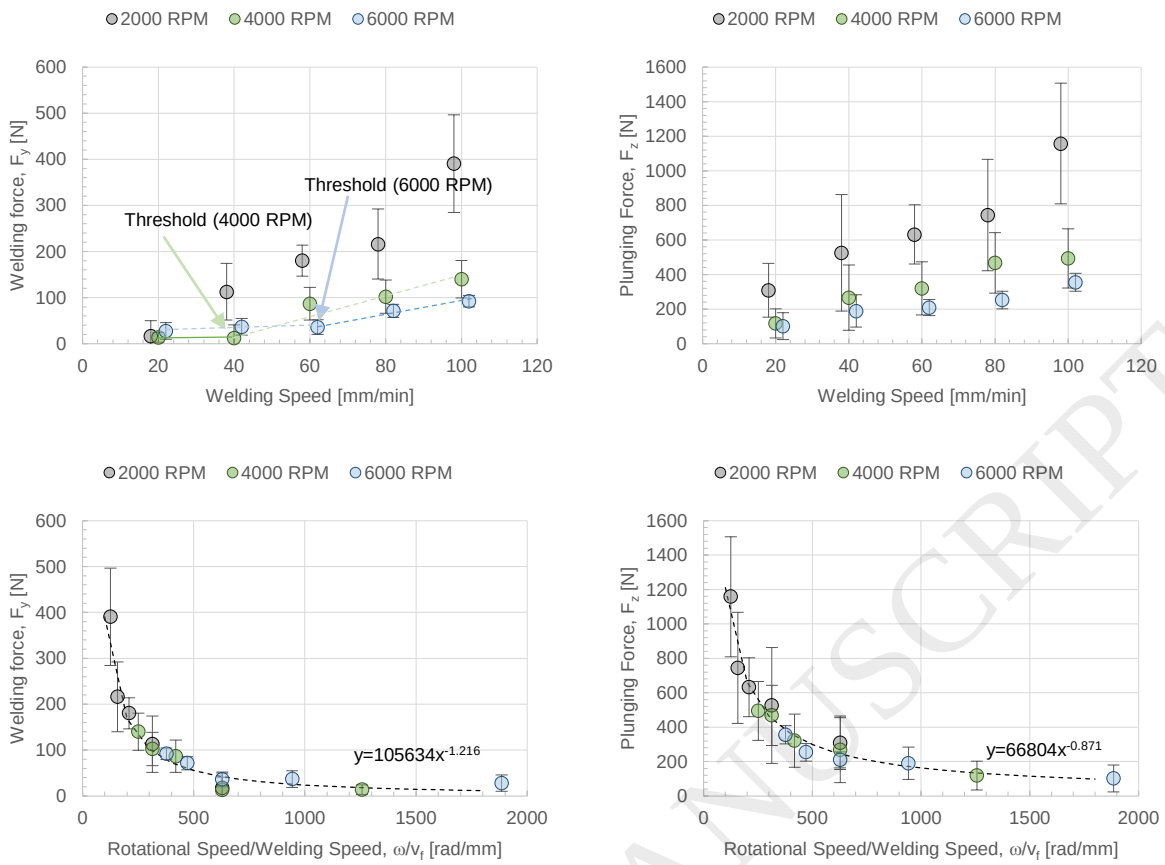

Fig. 8 Effect of the process conditions on average values of Fy and Fz.

Fig. 8c-d depict the variation of the welding and plunging force with rotational speed/welding speed ratio ω/v_f. This parameter is representative of the number of turns per unit length. These trends indicate that the processing loads follow an exponential decay with increasing ω/v_f. In addition, the average values of the processing loads are aligned along the same curve, regardless the value of tool rotation speed.

3.3.2 Analysis of torque and energy

The influence of the process parameters on the average values of the torque (M_z) and specific energy (E_s) is depicted in Fig. 9a and Fig. 9b, respectively. Even though the large error bars, Fig. 9a indicates that higher tool rotation speed required lower torque as greater temperatures were involved. The specific energy E_s was computed according to Eq. (2) and Eq. (3). The trends, reported in Fig. 9b, indicate that the tool rotation speed influenced E_s only marginally. Indeed, the increase of the tool rotation speed generally yielded a slight increase of E_s. On the other hand, E_s reduced significantly with the welding speed as this parameter determines the interaction time.

ACCEPTED MANUSCRIPT

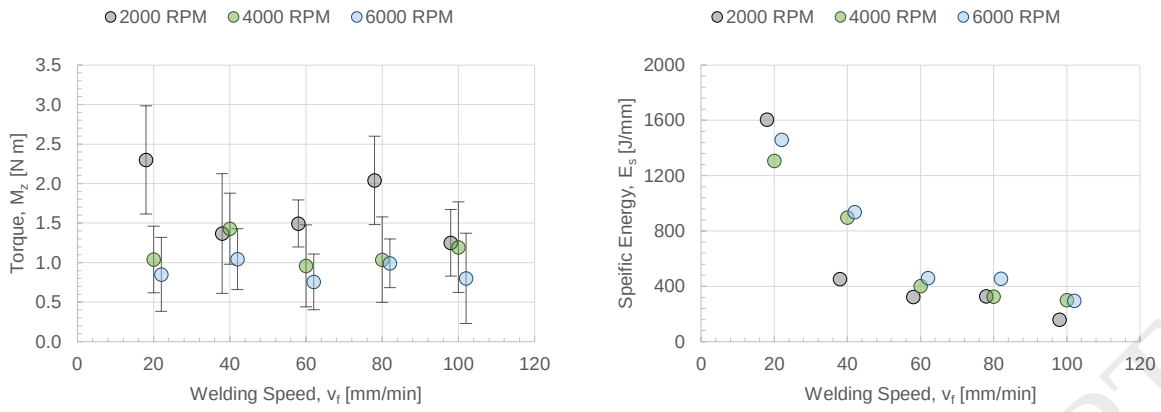

Fig. 9 Influence of process parameters on (a) torque and (b) specific energy.

3.4 Temperature distribution and variation with time

The variation of the emissivity of the PC surface with temperature (T) is reported in Fig. 10. The emissivity held almost constant at unity until T≤200 °C. Higher values of temperature involved a significant reduction in the emissivity (as shown by green marks). For T=360°C, the emissivity dropped to 0.6. Thus, the temperature measured above 360 °C must be considered only indicative as the emissivity was not measured. For these conditions, the value of 0.6 was assumed. On the other hand, for temperature below 360°C, the values of the emissivity reported in Fig. 10 were adopted. These data were used for IR temperature analysis during FSW experiments.

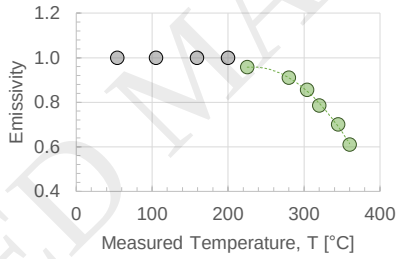

Fig. 10 Variation of emissivity with temperature.

Fig. 11 shows the variation of the temperature measured at the three points depicted in Fig. 1a for two different cases: (a) v_f=20 mm/min, ω=2000 RPM and (b) v_f=100 mm/min, ω=6000 RPM. The temperature data was reported against the position to simplify the comparison of curves regarding different welding speeds. The three data series concerning the points P1, P2 (Advancing Side) and P3 (Retracting Side) are characterized by similar features for both the conditions. Under v_f=20 mm/min, ω=2000 RPM condition, the temperature trend showed a special feature namely, the presence of narrow peaks. These peaks appeared in correspondence of the abovementioned circular rifts, as shown in Fig. 11a. On the other hand, when v_f=100 mm/min, ω=6000 RPM, no peaks were observed in the central region where steady state conditions fully developed. This came with a more uniform morphology of the weld surface, as shown in Fig. 11a. The presence/absence of the circular rifts was always consistent with the presence of temperature peaks for all the other cases analyzed.

ACCEPTED MANUSCRIPT

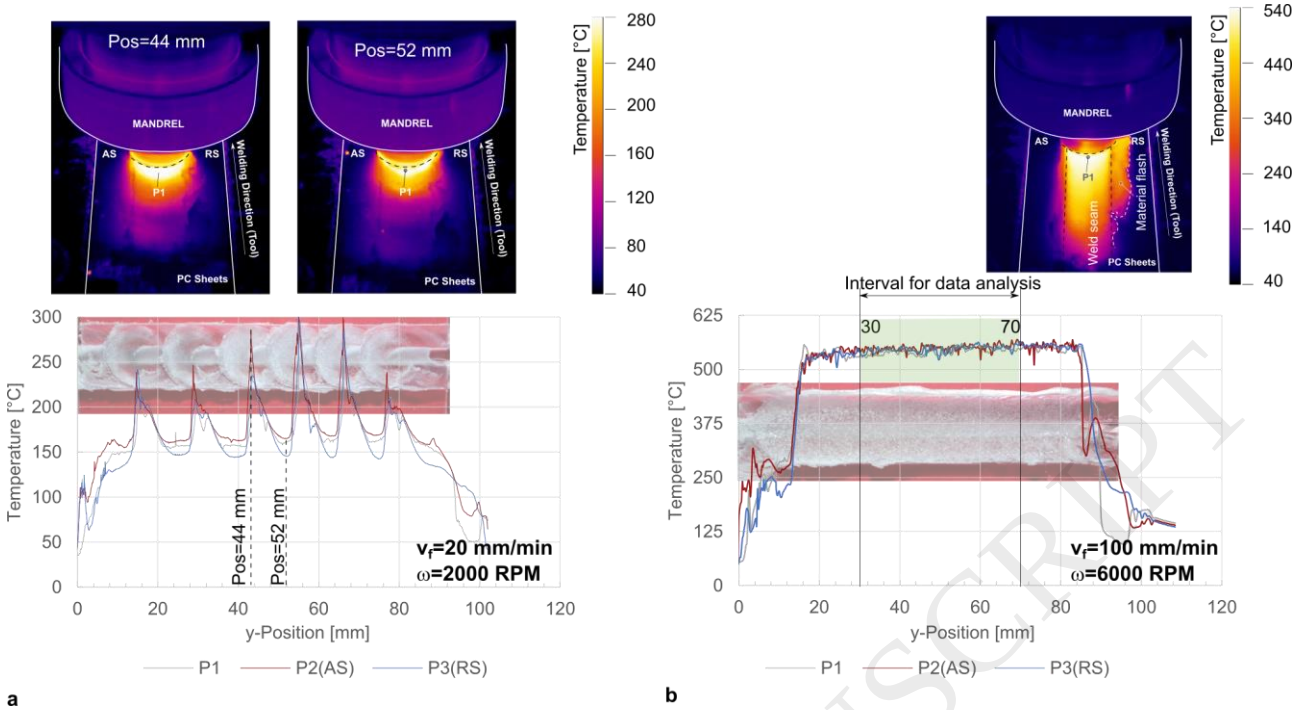

Fig. 11 Variation of temperature measured at different positions (P1, P2 and P3) with time for: (a) ω=2000, v_f=20 mm/min and (b) ω=6000, v_f=1000 mm/min.

The comparison of the curve trends from Fig. 11a concerning the points P2 (AS) and P3 (RS) indicate that the temperature in the advancing side was always higher than that observed in the retracting side especially in correspondence of the temperature valleys. This result is consistent with other experimental findings regarding FSW of metals and polymers. Similarly, when high welding speeds were adopted, the temperature of the advancing side rose more steeply than the retracting side as the process begins (up to a position of almost 10 mm). However, as the Built up edge developed, the temperature steeply increased and the difference between the AR and RS temperatures became negligible. This was observed in all processing conditions involving the formation of the BUE under the tool shoulder. This behavior was addressed to the milling action exerted by the tool.

Raw temperature data was analyzed in a region sufficiently distant from the entry and the exit positions (between positions 30 mm and 70 mm, as shown in Fig. 11b). This enabled to evaluate the influence of the processing parameters on the mean values and standard deviation of the temperature. These data were reported for the point P1 for sake of briefness (similar values were measured in correspondence of the other two points). Fig. 12 indicates that the average temperature increased for higher values of the tool rotation speed with the exception of the conditions v_f=20 mm/min. Under this condition, the temperature was slightly influenced by the tool rotation speed. The average temperature also increased with the welding speed. Such an increase was more marked up to v_f=60 mm/min, in correspondence of which the curves showed a knee. The reduction of the temperature increase from v_f=60 mm/min was addressed to higher amounts of heat exchange with the environment due to convection and radiation along with greater heat loss due to conduction with surrounding material and underlying steel plate. However, as in most cases (ω=4000 RPM and ω=6000 RPM) the temperature was higher than 360°C, some errors can be also addressed to unknown material emissivity. The error bars in Fig. 12 indicate the standard deviation of the temperatures measured over the “interval for data analysis”, depicted in Fig. 11b. The presence of the aforementioned temperature peaks viz. the presence of the circular rifts produced along the weld line determine an increase in the standard deviation of the temperature.

ACCEPTED MANUSCRIPT

On the other hand, for processing conditions characterized by uniform morphology and the absence of temperature peaks (e.g. v_f= 100 mm/min, ω=6000 RPM), the process was stable and it was characterized by narrow intervals of temperature variation. The amplitude of the standard deviation was consistent with the morphology of the joints. Actually, all the conditions involving the presence of the circular rifts were characterized by high values of the standard deviation. On the other hand, conditions promoting a uniform surface morphology were also characterized by low values of temperature deviation during the process. Fig. 12 also reports the tool condition after FSW pass (summarized in Table 3). The presence of degraded material under intermediate level of welding speed, as shown in Fig. 4b and e, and the absence of material degradation under higher welding speed Fig. 4c and f, are apparently inconsistent with the continuous rising of the material temperature with the welding speed (reported in Fig. 12). However, under high welding speeds, great part of degraded material was ejected from the weld and did not lie on the weld seam.

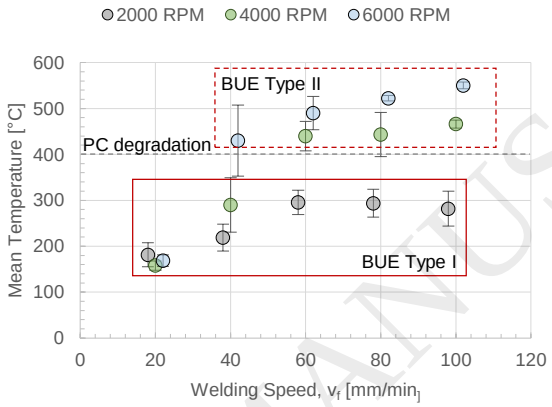

Fig. 12 Effect of tool rotation speed and welding speed on average and standard deviation of temperature (at point P1).

The influence of the welding speed on the mean temperature values reported in Fig. 12 is inconsistent with data reported in other researches concerning FSW. Derazkola and Simchi (2017) measured a reduction of the temperature with increasing the welding speed. The authors addressed such a reduction to the to the lower interaction time between the tool and the material. The argumentations reported by Derazkola and Simchi followed those concerning other processes such as laser treatments or even machining processes where the temperature increases with reducing the process speed (scanning/machining). This discrepancy is also clear when comparing the temperature trends with the pseudo "heat index" $w=\omega^2/v_f$. Arbegast and Hartley (1998) developed an empirical equation (reported in Eq. 4) that related the process temperature to the processing conditions.

$$\frac{T}{T_m} = K\left(\frac{\omega^2}{v_f \times 10^4}\right)^{\alpha} \qquad \text{Eq.4}$$

where α ranges between 0.04 and 0.06, and K between 0.65 and 0.75, and T_m (°C) is the melting point of the material. The temperature measurements performed on polycarbonate are in clear disagreement with this equation, since T should decrease with increasing v_f. Lambiase et al. (2018) developed a qualitative model that accounts the main heat exchanges influencing the material state during the process. The temperature within the stirred region and behind the tool depends on several aspects: the temperature of the material preceding the tool, the heat generation rate (due to friction between the tool and the material), the conductive heat towards the tool and the heat lost by conduction towards surrounding material. In addition, heat exchange by convection with the environment also occurs. Shi et al. (2015) investigated the influence of process parameters on heat generation rate during FSW of aluminum alloy. The results from the simulations

ACCEPTED MANUSCRIPT

indicated that the heat generation rate increased with increasing the welding speed. This was due to higher yield stress of the material being stirred. Nevertheless, the results of that study indicated a reduction of temperature with welding speed. However, in friction stir welding of polymers, the preheating of the material being stirred is confined to a narrow region just proceeding the tool (in the welding direction). This is due to the low thermal conductivity of these materials. For the same reason, poor conductive heat exchanges also develop towards the surrounding material, as can be observed in Fig. 11. When low welding speeds are adopted, the interaction time (which is proportional to the inverse of the welding speed) enables to preheat the material being stirred. The increase in temperature determines a significant material softening. When this material comes in contact with the tool, low interfacial contact stress and low contact forces develop, as reported in Fig. 8a and Fig. 8b. Thus, the heat produced by friction (which is proportional to the interfacial contact stress) is negligible. This results in lower material temperature within the stirred region and behind the tool, as schematized in Fig. 13a. On the other hand, when high processing speeds are adopted, the short interaction time leads to poor preheating of the material being stirred. Thus, high contact pressure develops at the tool/material interface, as shown in Fig. 8a and Fig. 8b. This is due to lower softening (higher interfacial contact stress) along with higher strain rate. This leads to great friction heat produced at the tool/material interface, despite the lower interaction time, as schematized in Fig. 13b.

During FSW, the different behavior of polymeric materials as compared to metals is due to the lower heat conductivity along with a greater sensitivity of their mechanical behavior to the temperature (e.g. steep reduction of the Young modulus as the temperature exceeds the Glass Transition Temperature Tg of the material). Thus, the model proposed by Arbegast and Hartley (1998) and similar models developed for metals cannot be applied to polymer materials as these models usually neglect the great variation of mechanical behavior of polymers with temperature.

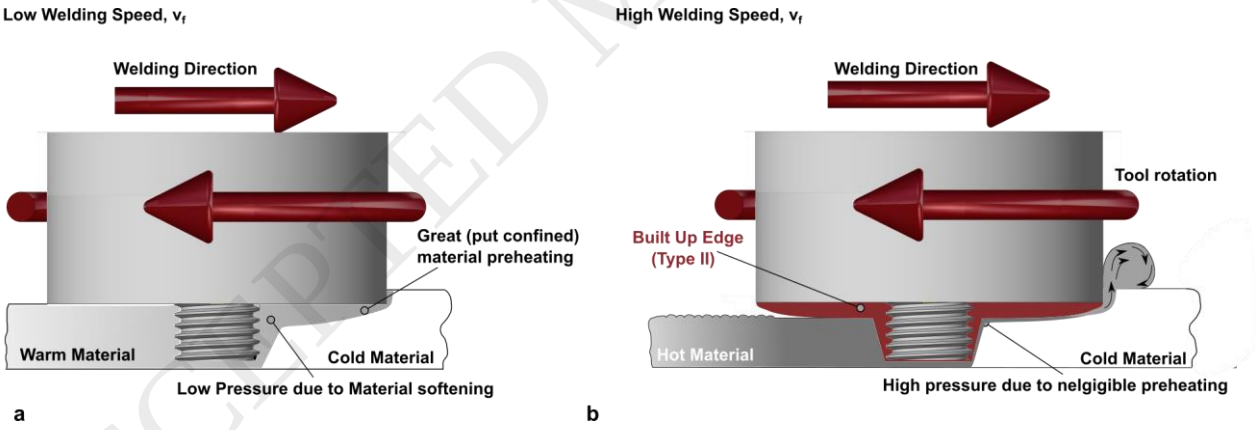

Fig. 13 Schematic of the effect of welding speed on temperature distribution and contact pressure.

The above-mentioned mechanisms could also explain the negligible influence of the tool rotation speed under low welding speed (v_f=20 mm/min). Actually, as the temperature of the material being stirred almost equals the Tg of the material, the friction heat becomes negligible regardless the tool rotation speed.

3.5 Mechanism of formation of the circular rifts

The presence of the above-mentioned circular rifts on the surface of the welds represents a clear defect. Thus, it should be avoided by means of the selection of proper process parameters or probably by means of closed-loop systems based on force and/or temperature

ACCEPTED MANUSCRIPT

control. An interpretation of the observations concerning the formation of the rifts is proposed in this section. During FSW of polycarbonate, the material often adhered to the pin and/or to the bottom face of the shoulder. This was also observed in FSSW of polycarbonate (2015). Generally, in metals cutting, the formation of the built up edge is due to high pressure and high temperature near the tool edge. Consequently, the presence of the build-up edge strongly depends on the processing conditions (welding speed and tool rotation speed). Under processing conditions leading to unsteady material flow, the development of the built up edge came with a steep increase of the welding load (F_y), as described in section 3.3.1. F_y is proportional to the flow stress of the material (in front of the tool) and to the cross section of the tool. The formation of the built-up edge determined the increase of the apparent cross section of the tool with consequent steep increase in the F_y component. The increase of the (apparent) tool dimension also determined the increase in the hydrostatic pressure under the tool. This resulted in the increase in the plunging load F_z.

When, processing conditions involving low-medium pressures (low welding speeds) were adopted, the material slightly adhered to the tool causing the increase in the F_y component. However, the BUE was rapidly ejected and it was backward extruded behind the tool. This caused a reduction in the hydrostatic pressure around the tool leading to a sudden drop of F_y and F_z, as shown in Fig. 6 and higher magnifications reported in Fig. 14. On the other hand, higher welding speeds induced high pressure in the welding direction (y-direction). This did not enable the reduction of the hydrostatic pressure under the tool leading to a constant built-up edge adhered around the pin surface and under the tool shoulder.

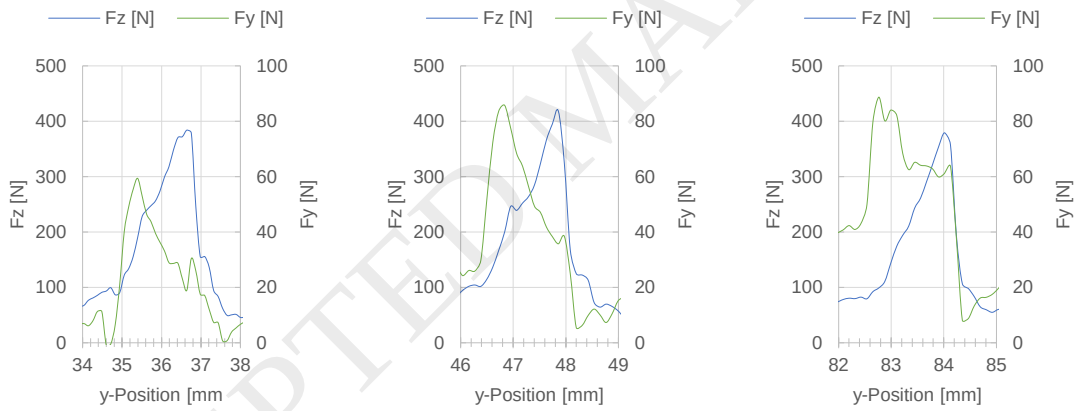

Fig. 14 High magnification of load trends revealing the formation of the BUE (ω=6000 RPM, v_f=20 mm/min).

3.6 Development of Built-up edge and milling action

The material flow was studied more in depth by means of experimental observations in front of the tool. To this end, a DSLR camera pointed on the material being stirred to capture the features of the material flow and to determine how it is influenced by the process parameters. Fig. 15 depicts a schematic of the conditions developing under high welding speeds. At the beginning, a thin flash of material is squeezed out from the front side of the tool. This material comes from the dark-grey region depicted in Fig. 15a. This region is compressed between the tool (both the pin and the shoulder) and the preceding material (depicted in light grey), which is much colder and consequently harder. As the process proceeds, the tool exerts high pressure on the material. This also comes with high temperatures development as higher normal pressure involves higher frictional heat. Part of the material within the dark-grey region adheres to the tool pin and under the tool shoulder leading to the formation of the Built up edge. Consequently, the tool exerts higher pressure on the material since its

ACCEPTED MANUSCRIPT

apparent dimension is increased by the presence of the BUE. This leads to a higher flow of material that is squeezed out from the front of the tool. However, this also comes with the above-mentioned milling effect as the front flash is not upset in the back of the tool (over the weld seam), leading to the material removal. The BUE develops very quickly when high welding speed are adopted; thus, the transition between the state schematized in Fig. 15a and that reported in Fig. 15b is relatively short.

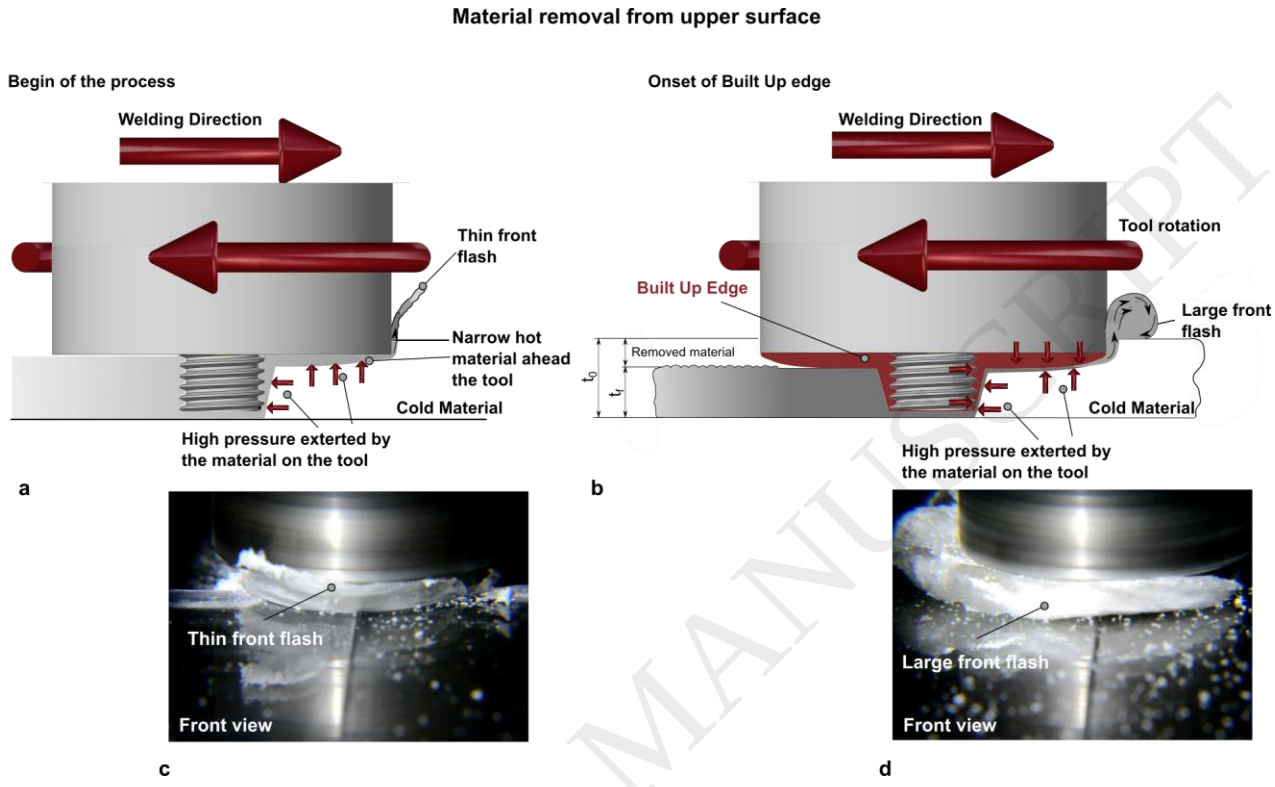

Fig. 15 Formation of BUE and milling effect.

4. Discussion

There is a widespread employment of polymers and their composites in many different applications. Common joining techniques such as adhesive bonding or fusion-based processes show several disadvantages due to performances limitations, process issue (costs, productivity, preprocessing requirements, etc.) and environmental impact. FSW process of thermoplastics is revealing as a valid alternative to get over these limitations. The study of the temperature distribution, the loads and the energy requirement would enable a better design of the process, tools and machines. In addition, the capability to forecast the development of critical conditions by means of load and/or temperature measurements could be exploited for development of "Intelligent Machines" in agreement with "Industry 4.0" philosophy.

This study was aimed at understanding how the temperature and processing loads are influenced by process parameters while performing FSW on polycarbonate sheets. The study involved relatively high welding speeds. The superficial morphology of the welds and the correlation between development of critical conditions leading to superficial defects and temperature and load signals were investigated. The results clarified the influence of the process parameters on processing temperatures and loads. Two types of defects were identified on FSW welds. Under low welding speeds, the welds were mainly affected by the presence of circular rifts that were produced due to unsteady process conditions. Under high welding speeds, high temperature (even exceeding the degradation temperature of the polymer) and pressure conditions resulted in the formation of built-up edge (BUE) under the tool shoulder. The presence of the BUE modified the effective geometry of the tool and increased the amount of material squeezing in front of the tool leading to the "milling

ACCEPTED MANUSCRIPT

action" on the weld path. The comparison among morphological aspects and the acquired signals indicated that both temperature and load signals can be used to predict the development of defects such as circular rifts as well as steady conditions. A mechanism of formation of these defects was proposed.

However, a validation of the proposed explanation is still required. Thus, a possible improvement to understand more comprehensively the mechanism of formation of the aforementioned defects would be the development of a numerical model involving both thermal and mechanical aspects. In addition, further experimental study is needed to determine the influence of other processing parameters (the geometry, dimension and topology of the tool, the plunging depth, the tilt angle and the tool material) on the development of the abovementioned defects and built-up edge formation. These parameters can significantly modify the pressure on the material being stirred, and consequently the processing loads, the temperature and morphology of the welds. These aspects will be treated in upcoming studies. Furthermore, as the adoption of high welding speeds would involve an increase in the productivity and the reduction of the specific energy, particular attention should be paid to avoid the formation of BUE under such conditions.

Despite other processes (machining, laser treatments), this paper clarifies that for FSW process of polymers the temperature increases with the welding speed. This is due to the increase in the contact and hydrostatic pressure that promoted higher frictional heat. These results provide a new process understanding that immediately drive towards a new question: "How the process could be modified in order to reduce the temperature at higher welding speeds?"

5. Conclusions

Butt welds are produced on polycarbonate sheets by means of Friction Stir Welding process. The variation of the processing loads, temperature and the macroscopic morphology of the welds is investigated experimentally. The effects of the welding speed and tool rotation speed are investigated.

The morphology of the welds showed two types of macroscopic defects. Low welding and tool rotation speeds led to the formation of periodic circular rifts. The development of the circular rifts was due to low pressure exerted by the tool on the material, which resulted in the development of periodic/unstable processing conditions. Both loads and temperature measurements were capable to underlie the onset of such periodic trends. Thus, these measurements can be used to predict and even avoid the onset of unsteady conditions.

Temperature measurements, performed by means of IR thermography, indicate that higher welding speed involves higher temperatures within the stirred region. Prior investigations showed an opposite trend. The increase of temperature with the welding speed is addressed to the increase of the contact pressure that in turn comes with an increase in the frictional heat. Welding speed higher than 60 mm/min resulted in thermal degradation of the polycarbonate.

High welding speeds also come with great amount of material removal from the upper surface of the sheets. This was due to the material adhesion under the tool shoulder (Built-up edge) that exerted a milling action of the surrounding material. This phenomenon was due to the high pressure exerted on the tool, along with high temperatures of the stirred region.

ACCEPTED MANUSCRIPT

Acknowledgements

The authors would like to thank Mrs. F. Ferrante and Mr. G. Spagnoli, (DIIIE, University of L'Aquila) for their contribution for characterization tests.

References

Aghajani Derazkola, H., Simchi, A., 2018a. Effects of alumina nanoparticles on the microstructure, strength and wear resistance of poly(methyl methacrylate)-based nanocomposites prepared by friction stir processing. J Mech Behav Biomed Mater 79, 246-253.
Aghajani Derazkola, H., Simchi, A., 2018b. Experimental and thermomechanical analysis of the effect of tool pin profile on the friction stir welding of poly(methyl methacrylate) sheets. Journal of Manufacturing Processes 34, 412-423.
Arbegast, W.J., Hartley, P.J., 1998. Friction Stir Weld Technology Development at Lockheed Martin Michoud Space System - An Overview, International conference; 5th, Trends in welding research. ASM International, Pine Mountain; GA, pp. 541-546.
Azarsa, E., Mostafapour, A., 2013. On the feasibility of producing polymer–metal composites via novel variant of friction stir processing. Journal of Manufacturing Processes 15, 682-688.
Bagheri, A., Azdast, T., Doniavi, A., 2013. An experimental study on mechanical properties of friction stir welded ABS sheets. Materials & Design 43, 402-409.
Banjare, P.N., Sahlot, P., Arora, A., 2017. An assisted heating tool design for FSW of thermoplastics. Journal of Materials Processing Technology 239, 83-91.
Bozkurt, Y., 2012. The optimization of friction stir welding process parameters to achieve maximum tensile strength in polyethylene sheets. Materials & Design 35, 440-445.
Derazkola, H., Simchi, A., 2017. Experimental and thermomechanical analysis of friction stir welding of poly(methyl methacrylate) sheets.
Elyasi, M., Derazkola, H.A., 2018. Experimental and thermomechanical study on FSW of PMMA polymer T-joint. The International Journal of Advanced Manufacturing Technology 97, 1445-1456.
Eslami, S., Mourão, L., Viriato, N., Tavares, P.J., Moreira, P.M.G.P., 2018. Multi-axis force measurements of polymer friction stir welding. Journal of Materials Processing Technology 256, 51-56.
Gao, J., Li, C., Shilpakar, U., Shen, Y., 2016. Microstructure and tensile properties of dissimilar submerged friction stir welds between HDPE and ABS sheets. The International Journal of Advanced Manufacturing Technology.
Huang, Y., Meng, X., Xie, Y., Wan, L., Lv, Z., Cao, J., Feng, J., 2018. Friction stir welding/processing of polymers and polymer matrix composites. Composites Part A: Applied Science and Manufacturing 105, 235-257.
Lambiase, F., Paoletti, A., Di Ilio, A., 2015. Mechanical behaviour of friction stir spot welds of polycarbonate sheets. The International Journal of Advanced Manufacturing Technology 80, 301-314.
Lambiase, F., Paoletti, A., Di Ilio, A., 2017a. Friction spot stir welding of polymers: control of plunging force. The International Journal of Advanced Manufacturing Technology 90, 2827-2837.
Lambiase, F., Genna, S., Leone, C., Paoletti, A., 2017b. Laser-assisted direct-joining of carbon fibre reinforced plastic with thermosetting matrix to polycarbonate sheets. Optics & Laser Technology 94, 45-58.
Lambiase, F., Paoletti, A., Di Ilio, A., 2018. Forces and temperature variation during friction stir welding of aluminum alloy AA6082-T6. The International Journal of Advanced Manufacturing Technology 99, 337-346.
Mendes, N., Loureiro, A., Martins, C., Neto, P., Pires, J.N., 2014a. Effect of friction stir welding parameters on morphology and strength of acrylonitrile butadiene styrene plate welds. Materials & Design 58, 457-464.
Mendes, N., Loureiro, A., Martins, C., Neto, P., Pires, J.N., 2014b. Morphology and strength of acrylonitrile butadiene styrene welds performed by robotic friction stir welding. Materials & Design 64, 81-90.
Moreno-Moreno, M., Macea Romero, Y., Rodríguez Zambrano, H., Restrepo-Zapata, N.C., Afonso, C.R.M., Unfried-Silgado, J., 2018. Mechanical and thermal properties of friction-stir welded joints of high density polyethylene using a non-rotational shoulder tool. The International Journal of Advanced Manufacturing Technology 97, 2489-2499.
Panneerselvam, K., Lenin, K., 2014. Joining of Nylon 6 plate by friction stir welding process using threaded pin profile. Materials & Design 53, 302-307.
Sahu, S.K., Mishra, D., Mahto, R.P., Sharma, V.M., Pal, S.K., Pal, K., Banerjee, S., Dash, P., 2018. Friction stir welding of polypropylene sheet. Engineering Science and Technology, an International Journal 21, 245-254.
Shi, L., Wu, C.S., Liu, H.J., 2015. The effect of the welding parameters and tool size on the thermal process and tool torque in reverse dual-rotation friction stir welding. International Journal of Machine Tools and Manufacture 91, 1-11.

ACCEPTED MANUSCRIPT

Simões, F., Rodrigues, D.M., 2014. Material flow and thermo-mechanical conditions during Friction Stir Welding of polymers: Literature review, experimental results and empirical analysis. Materials & Design 59, 344-351.
Vijendra, B., Sharma, A., 2015. Induction heated tool assisted friction-stir welding (i-FSW): A novel hybrid process for joining of thermoplastics. Journal of Manufacturing Processes 20, 234-244.

ACCEPTED MANUSCRIPT

ACCEPTED MANUSCRIPT

Table 1 Main Mechanical properties of Polycarbonate (LEXAN) at room temperature

Young's Modulus [GPa]	Yield Strength [MPa]	Elongation at rupture [%]
2.1	60	98

Table 2 Experimental plan of FSW tests.

Level	Tool Rotation Speed, ω [RPM]	Welding Speed, v_f [mm/min]
I	2000	20
II	4000	40
III	6000	60
IV		80
V		100

Table 3 Effect of process conditions of the type of Built-up Edge

	Welding Speed, v_f [mm/min]				
Tool Rotation Speed, ω [RPM]	20	40	60	80	100
2000	Type I	Type I	Type I	Type I	Type I
4000	Type I	Type I	Type II	Type II	Type II
6000	Type I	Type I	Type II	Type II	Type II

ACCEPTED MANUSCRIPT